Oxidation of Metals, Vol. 47, Nos. 3/4, 1997

High-Temperature Oxidation Behavior of Laser-Surface-Alloyed Incoloy-800H with Al

Alejandro Gutiérrez* and Juan de Damborenea*

Received May 3, 1996; revised July 15, 1996

The high-temperature oxidation resistance of laser-surface-alloyed Incoloy-800H with Al has been investigated. Several samples have been exposed to 1000°C in air and subsequently analyzed by optical microscopy, SEM, and electron microprobe X-ray fluorescence spectroscopy in order to determine their microstructure and composition. The results show that the laser-treated materials have a considerably higher oxidation resistance than the nontreated materials due to the formation of an Al-rich layer close to the surface, which acts as a barrier against oxygen diffusion into the bulk.

KEYWORDS: laser surface alloying; aluminum; superalloys; oxidation; microstructure.

INTRODUCTION

Several processes influencing materials lifetime, such as wear or corrosion, take place at the surface. Their effect can thus be reduced by changing either the composition or microstructure of the outer part of the material. From an economical point of view, modifying only the surface is usually cheaper than using a bulk material with the same characteristics as the modified surface. From an engineering point of view, materials with good bulk mechanical properties may have a relatively low wear or corrosion resistance, which can be improved by modifying their surface. The modified material conserves its good bulk mechanical properties while improving its corrosion and wear resistance.[1,2]

*Departamento de Corrosión y Protección, Centro Nacional de Investigaciones Metalúgicas (CENIM), CSIC, Avda Gregorio del Amo 8, E-28040 Madrid, Spain.

0030-770X/97/0400-0259$12.50/0

Laser-surface modification of metallic materials constitutes a very good method for improving their surface properties due to the high power densities involved in the process.[3,4] The extremely high heating and cooling rates produce new phases with considerable grain refinement, which may improve the corrosion resistance of the treated material.[5,6] Laser-surface treatment can either induce microstructural changes at the surface without changing its composition (laser-surface hardening or melting[6]), or change both the surface microstructure and composition (laser-surface alloying and cladding).[7–9]

The iron-based superalloy Incoloy-800H combines good strength and a relatively good resistance to oxidation and carburation at high temperatures due to the formation of a protective Cr_2O_3 scale at the surface.[10] The protectiveness of this scale, however, drastically decreases for temperatures above the working temperature of the material (~750°C), especially in the presence of carburizing gases.[11] On the other hand, Al_2O_3 scales can reduce oxidation rates at high temperatures up to a factor 8,[12] and they may form at low oxygen potentials, where Cr_2O_3 scales are difficult to form. An addition of Al to the surface of Incoloy-800H would improve its resistance to oxidation at high-temperatures, as well as its resistance against carburization and sulfidation.

In the present work, the high-temperature oxidation behavior of laser-surface-alloyed Incoloy-800H with Al has been investigated. Several samples have been isothermally oxidized in air at 1000°C for different time intervals and subsequently characterized by scanning electron microscopy (SEM), optical microscopy, and electron microprobe X-ray fluorescence analysis. The results indicate a considerable improvement in the oxidation resistance of the treated alloy as compared with the untreated material.

EXPERIMENTAL DETAILS

The iron-base superalloy Incoloy-800H, with nominal composition (wt%) Fe 45.36, Ni 30.78, Cr 20.0, Co 0.87, Mn 0.71, Si 0.52, Cu 0.49, and Ti 0.33, was used as the substrate alloy. Several discs, 5-mm thick, were cut from a 60-mm diameter rod. Laser-surface alloying was carried out by the powder-injection method.[6,13] Pure aluminum powder (99.9%) was fed by means of an argon stream into the molten pool produced by the laser on the substrate. A powder-feed unit equipped with a flow balance was used to control the Al powder feed rate, which was set at 3 g/min. The laser employed was a CO_2 continuous wave laser (Spectra Physics) operated in multimode beam, with an output power of 5000 kW and a spot area on the surface of 64 mm^2. The substrate disc was sand blasted before laser treatment in order to reduce losses caused by reflectivity. The laser beam was scanned

onto the samples by moving them at a constant traverse speed of 800 mm/min. Both traverse speed and Al powder feed rate determine the main properties of the treated surface. A previous characterization study of samples prepared with different values of these parameters showed that those used in the present work (800 mm/min and 3 g/min) produce the best quality coatings.[14]

Four laser tracks were made on each disc. After laser treatment, several samples ($15 \times 5 \times 5$ mm) were cut from the disc, each one including two track sections. Samples were then introduced into a furnace at 1000°C in an air atmosphere for different time intervals. In order to expose only the laser-treated side of the samples to air, all other sides were previously covered with a high-temperature ceramic clay. Once this ceramic had cured, six samples were isothermally oxidized at 1000°C for 25 hr, 50 hr, 100 hr, 200 hr, 480 hr and 1000 hr, respectively. After this oxidation, samples were extracted from the furnace and the ceramic shell removed. The cooling rate was approximately 1 K/s. Microstructure and composition of the tracks as compared to the substrate were determined by optical microscopy, scanning electron microscopy (SEM), and electron microprobe X-ray fluorescence analysis. Metallographic observations were carried out on cross sections of the material, which were previously polished and chemically attacked in order to emphasize the different metallographic phases. SEM pictures and fluorescence spectra were obtained using a commercial JEOL-JXA 840 system with 15 keV incident electron energy. Element-selective mappings were obtained by scanning the electron beam across a sample region while detecting the X-ray fluorescence signal at the characteristic energy of the corresponding element.

EXPERIMENTAL RESULTS

Figure 1 shows a top view of four samples after different high-temperature oxidation times. In all cases the central part corresponds to the substrate alloy, and at both sides two laser tracks are visible. Figure 1a corresponds to a sample without any high-temperature oxidation treatment. The good surface finish of the tracks and their metallic aspect can be observed. Figure 1b corresponds to a sample oxidized at 1000°C for 25 hr. The metallic appearance of the tracks has disappeared, transforming into an opaque, light gray tone, typical of some ceramic materials, and contrasting with the darker color of the central region, which resembles a metallic oxide (probably a mixture of Fe, Ni, and Cr oxides). The scale on this oxidized central part has spalled from the base alloy due to the different thermal contractions of the oxide layer and the bulk alloy during cooling of the samples to room temperature. This is evidenced by comparing Fig. 1b, where the spalled oxide

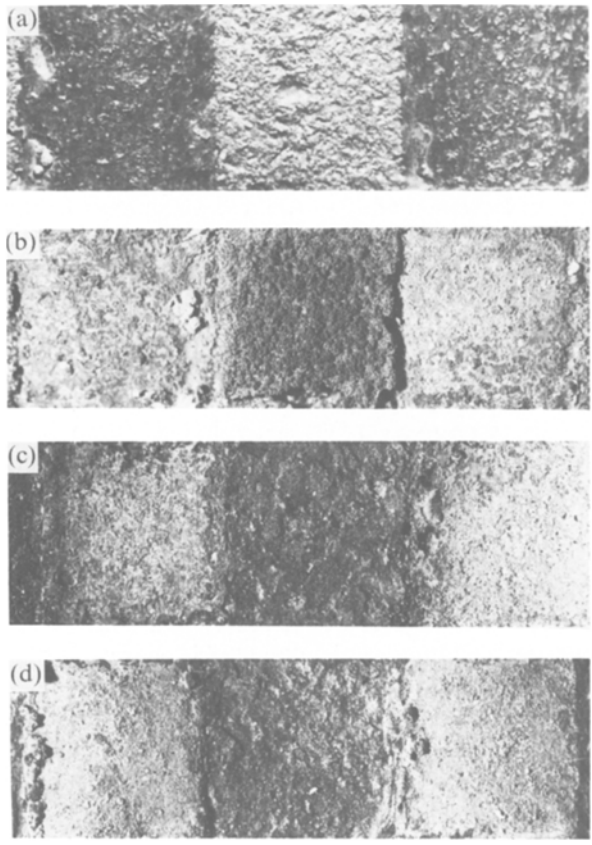

Fig. 1. Top view of four laser-surface-alloyed samples after different high-temperature oxidation treatments: (a) no high-temperature oxidation, (b) 25 hr at 1000°C, (c) 100 hr at 1000°C, and (d) 480 hr at 1000°C.

scale has been allowed to remain on the sample after spallation, with Fig. 1c, where the scale has already dropped off. On the other hand, no signs of scale spallation are observed on the laser tracks. Figures 1c and 1d correspond to samples oxidized at 1000°C for 100 hr and 480 hr, respectively, and are shown after the oxide layer on the nontreated alloy has spalled. Since spallation occurs at the first cooling stages, new oxide scales develop below the spalled scale, which results in a final oxidized surface. The central part shows a gradually deeper profile as compared to the laser tracks, indicating a severe corrosion process of the base alloy which apparently does not affect the laser treated surfaces.

In Figure 2, metallographic cross sections of different samples at regions close to one of the laser-track boundaries are shown. Figure 2a corresponds to a sample without any high-temperature oxidation treatment. It consists basically of a solid solution of Fe, Ni, and Cr, with Al, forming equiaxed grains. Two additional phases, with higher Al contents, are also present in form of precipitates. The first one is located at the grain boundaries, and, according to a previous study,[14] it can be assigned to Fe–Al intermetallic compounds. The second phase, with the highest Al content, is found inside the grains, and is assigned to different Cr–Fe–Al compounds.[14] Despite the abrupt pool/substrate interface, without intermediate mixed zone (similar to laser surface cladded coatings), the alloyed coatings showed very good adherence. Note the homogeneity and grain refining of the laser-treated zone.

As can be observed in Fig. 2b, the grain structure of the nonheat-treated sample disappears even after the shortest oxidation time, i.e., 25 hr, transforming into a dendritic structure with two main phases and some secondary phases. The reason of such drastic transformation might be the precipitation of stable phases that were not allowed to appear due to the extremely fast cooling rate that follows the laser treatment. The dendritic size increases with oxidation time, as can be observed in the samples oxidized for 100 hr (Fig. 2c), 200 hr (Fig. 2d), and 1000 hr (Fig. 2e). However, the most significant feature observed upon increasing oxidation time is the formation and subsequent growth of a barrier surrounding the laser-alloyed zone, and more appreciably at the surface, formed by small black aggregates. As it will be shown below, these aggregates are rich in Al_2O_3. In Fig. 2b (25 hr oxidation), the first stages of the barrier formation can be observed, whereas in Fig. 2c (100 hr oxidation), the barrier becomes perfectly clear. The formation of this barrier involves diffusion of some components from the dendritic phase, creating a precipitate-free zone below the barrier. This zone grows as the thickness of the barrier increases, being thickest for the maximum oxidation time (Fig. 2e). It is interesting to emphasize the morphological differences between the surface and the alloyed-zone/substrate interface. First, the barrier is much thicker at the surface than at the interface, forming a continuous layer for the longest oxidation times (Figs. 2d and 2e). A second difference is the existence of an outer layer of material above the barrier at the surface, whereas at the interface the barrier constitutes the outer border. The surface external layer is not visible in all cases since, due to its different thermal expansion coefficient as compared to the barrier, it is partly detached from the sample when it is cooled from 1000°C to room temperature after oxidation. Another difference between surface and interface, observed in Fig. 2e, is the formation at the former of an intermediate region between the precipitate-free zone and the barrier. This region is rich

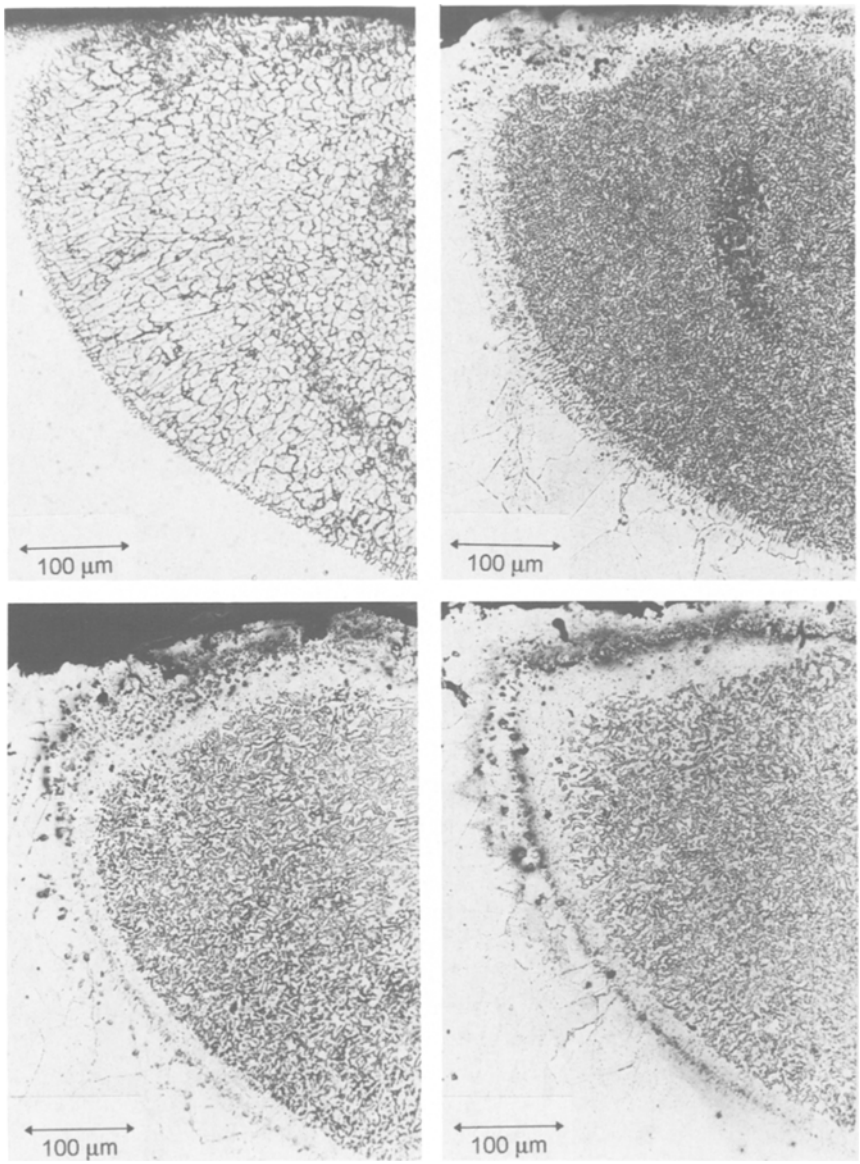

Fig. 2. Cross section of the laser-track boundary region of several samples after different oxidation periods at 1000°C: (a) no high-temperature oxidation, (b) 25 hr, (c) 100 hr, (d) 200 hr, and (e) 480 hr. The image magnification is ×20 for (a), (b), (c), and (d), and ×10 for (e).

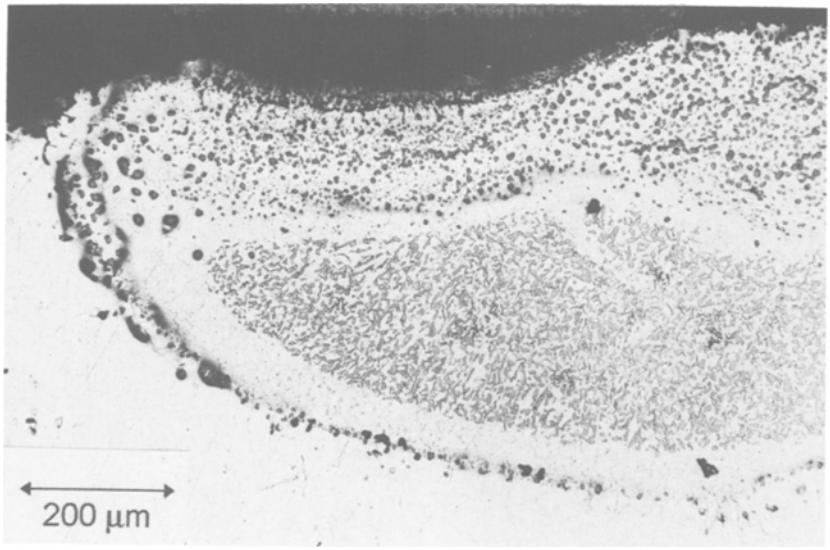

Fig. 2. Continued.

in black aggregates similar to those forming the barrier, but with a larger separation between them.

The evolution of the inner dendritic structure of the laser-treated zone with oxidation time is shown in Fig. 3. Figures 3a, 3b, 3c, and 3d correspond to oxidation times of 25 hr, 50 hr, 100 hr, and 200 hr, respectively. As already observed in Fig. 2, an increase in the dendritic size with oxidation time is evident, with a growth of approximately a factor 3 between the dendrites in Fig. 3a (25 hr) and those in Fig. 3d (200 hr). Additionally to the dendritic phase and the matrix, other phases in the form of precipitates can be observed in Fig. 3. In order to carry out a more detailed analysis and to identify all phases observed in the metallographic images, SEM examinations and electron microprobe X-ray fluorescence spectroscopy measurements with element-sensitive mapping were performed. Figure 4 shows a SEM image of the region close to the surface of the sample oxidized at 1000°C for 25 hr, as well as the corresponding Al, Cr, Fe, and Ni maps. The SEM image (Fig. 4a) presents basically the same features observed by optical microscopy, i.e., the initial stages of the formation of the barrier, visible as a layer of black aggregates close to the surface, regions above and below the barrier with lack of dendritic phases, and the region below them with the dendritic structure. In this case, however, two different zones can be distinguished in the dendritic region. The upper zone, close to the barrier, seems to consist only of one dendritic structure and the matrix, whereas the

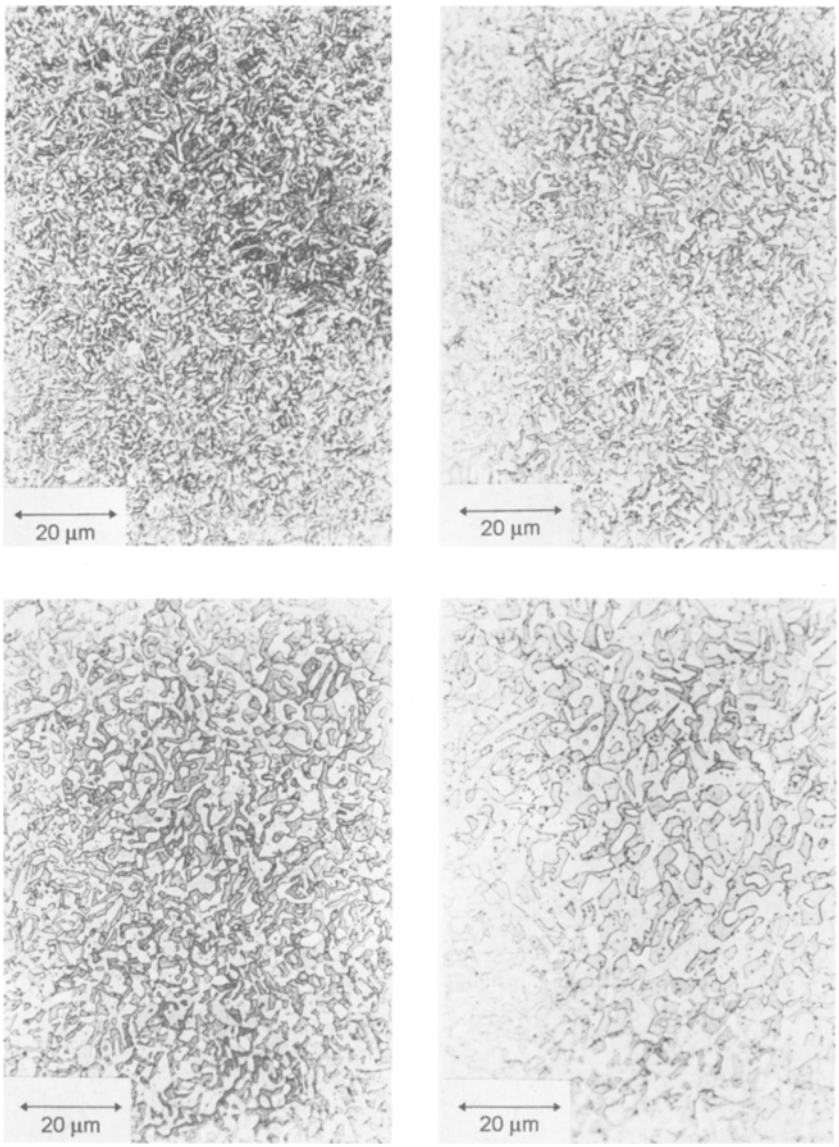

Fig. 3. Detail of the dendritic phase for several samples after different oxidation periods at 1000°C: (a) 25 hr, (b) 50 hr, (c) 100 hr, and (d) 200 hr. The image magnification is ×100.

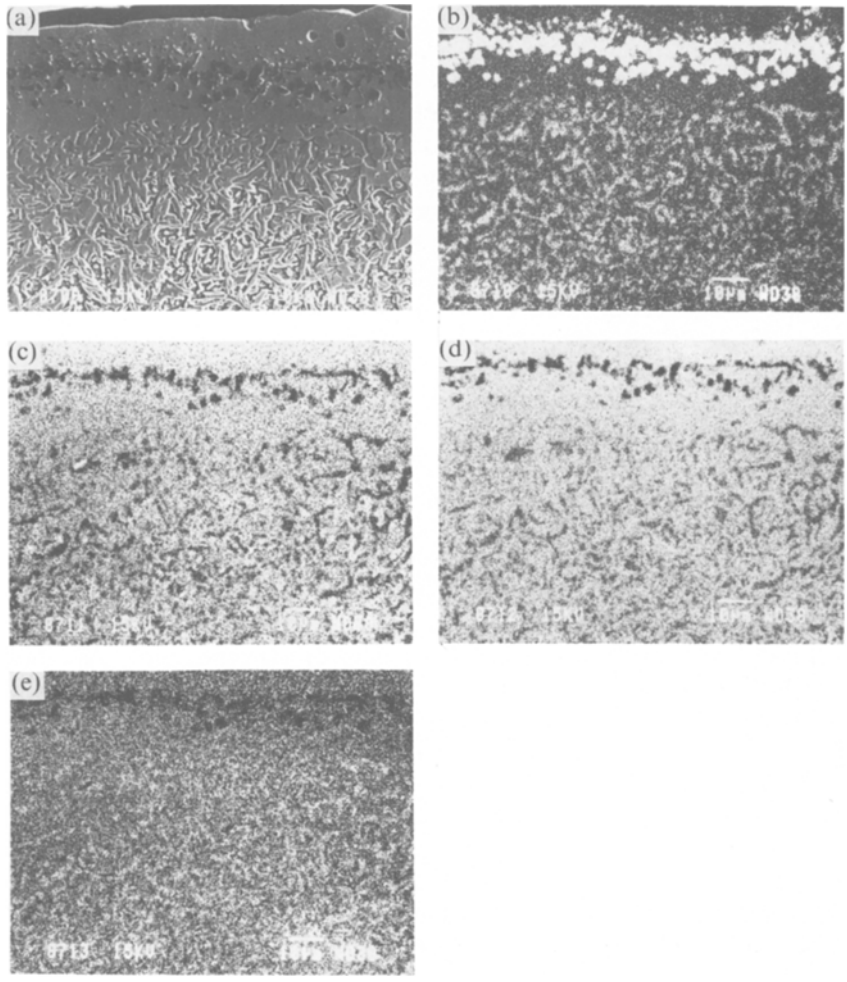

Fig. 4. SEM image (a) and the corresponding Al (b), Cr (c), Fe (d), and Ni (e) elemental maps of the surface region of a sample oxidized at 1000°C for 25 hr.

lower zone has an additional phase, that appears brighter, which alternates with the phase observed in the upper zone. The apparently lighter appearance of this second structure is due to its higher emission of secondary electrons, which indicates that it is composed of heavier atomic elements than the first dendritic structure. This point will be confirmed below. Figures 4b, 4c, 4d, and 4e correspond to Al, Cr, Fe, and Ni maps of the same region as that shown in Fig. 4a. It is evident from Fig. 4b that the barrier close to the surface consists mainly of aluminum, with very little or no contribution

from the rest of the main elements. The matrix appears uniform throughout the whole region, with Fe and Cr as main constituents, and a smaller contribution from Al and Ni. These two elements, probably in the form of intermetallic compounds, are the main constituents of the dendritic grains, as can be observed in Figs. 4b and 4e, with a very little contribution from Fe and Cr (Figs. 4c and 4d). Though it cannot be distinguished in the figure, the second dendritic phase observed in the lower zone of the SEM image corresponds to an Fe–Cr phase, as will be shown below.

In Fig. 5, a SEM image of the sample oxidized for 100 hr, together with the corresponding Al, Cr, Fe, and Ni maps, are shown. The thickness of the barrier has increased notably with respect to Fig. 4, and some aggregates have started to merge, forming a more continuous structure. Some additional Al-rich aggregates are observed above the barrier, with a more irregular elongated shape, and with larger size. These aggregates reach in some cases the external surface, being in contact with the atmosphere. As already discussed, the topmost layer of material above the barrier spalled during cooling of the sample to room temperature. The presence of Al-rich aggregates in this zone, similar to those forming the barrier, could attenuate this process. Another difference with respect to Fig. 4 is the absence in this case of the second dendritic phase in the SEM image. It will be shown that it gradually disappears with oxidation time. Concerning the element maps, they look quite similar to those in Fig. 4, except for the mentioned changes at and above the barrier, the larger size of the dendritic phase, and the appearance of Cr-rich aggregates, visible in Fig. 5c.

In Fig. 6, a SEM image and the corresponding element maps of the interface region of the same sample shown in Fig. 5 are shown. The main differences with respect to the surface are the smaller thickness of the barrier and the precipitate-free zone between barrier and dendritic zone, as well as the presence of Cr-rich aggregates in the barrier, and not only in the dendritic region, as was the case at the surface. Note also the smaller size of the dendrites with respect to the surface, which is probably associated with the smaller thickness of the barrier. Another interesting point is that the composition of the matrix does not seem to defer much from the substrate, since no discontinuities are observed in any of the element maps at the interface between the substrate and the laser-treated zone.

DISCUSSION

The aim of the present work was to study the improvement in the high-temperature oxidation resistance of the iron-base superalloy Incoloy-800H after laser-surface alloying with Al. The resulting alloyed material has a mean Al content of 16%, as determined by X-ray fluorescence analysis over

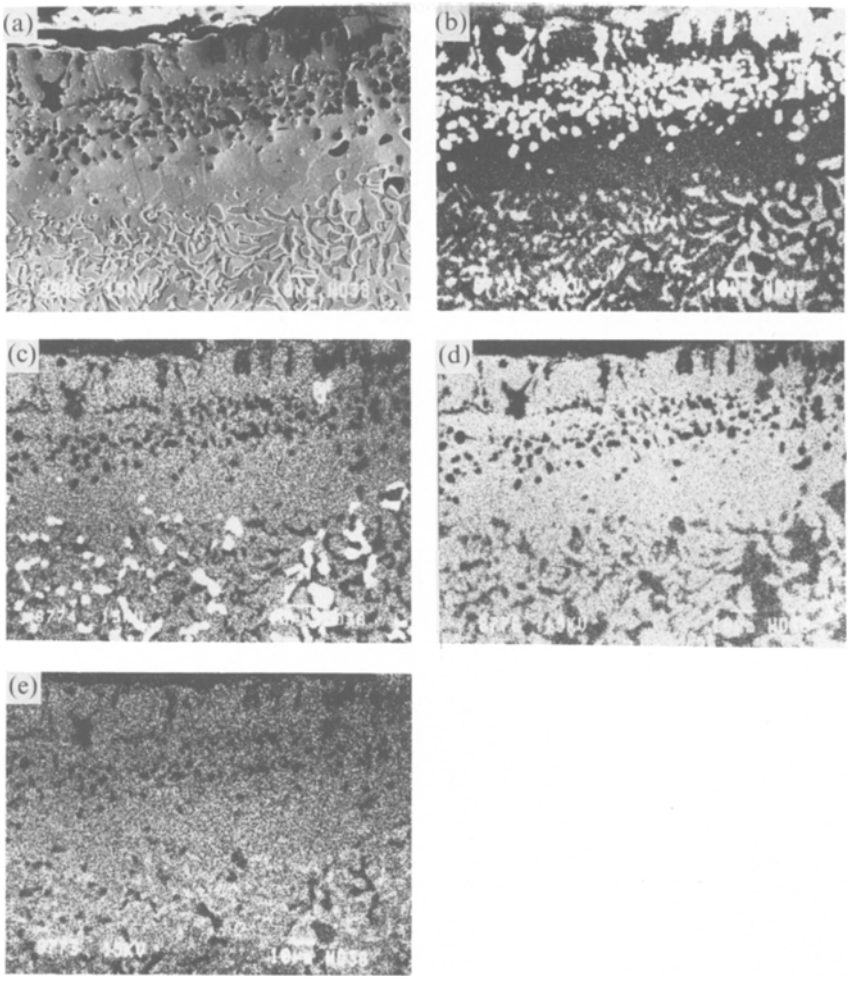

Fig. 5. SEM image (a) and the corresponding Al (b), Cr (c), Fe (d), and Ni (e) elemental maps of the surface region of a sample oxidized at 1000°C for 100 hr.

a broad area on the sample. This value should considerably increase the corrosion resistance of the base material.[15] In order to make accelerated oxidation tests, the laser-treated samples were exposed to air at 1000°C, a temperature well above the working temperature of the base alloy (approx. 300°C above).[10] The first consequences of such a severe treatment can be observed in Fig. 1. After 480 hr oxidation, a thick oxide layer has grown on the Incoloy-800H substrate surface, which, after cooling to room temperature, and due to the different thermal expansion coefficient of the oxide with

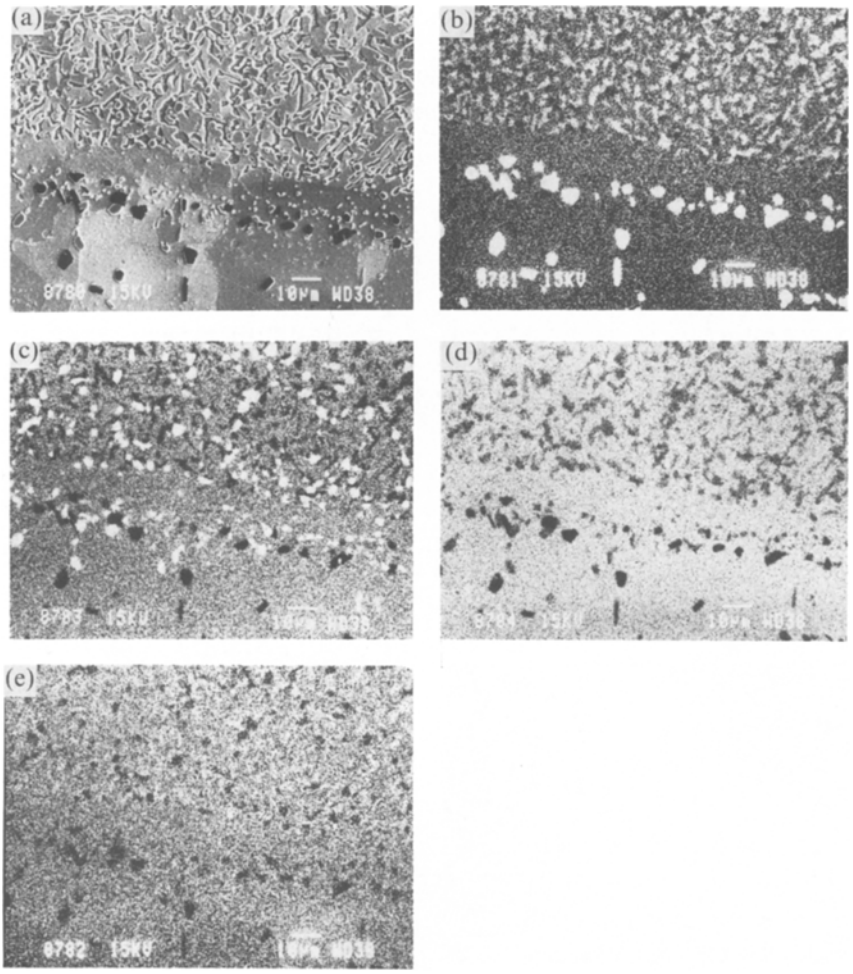

Fig. 6. SEM image (a) and the corresponding Al (b), Cr (c), Fe (d), and Ni (e) elemental maps of the interface region of a sample oxidized at 1000°C for 100 hr.

respect to the substrate, has spalled off from the sample (see Fig. 1d). This poor adherence of the oxide layer, as well as deep intergranular oxidation, have been previously reported.[7] On the other hand, the laser-treated sections do not seem to have been affected by such a severe corrosion process. From this first visual inspection, it is evident that the present laser treatment on Incoloy-800H greatly improves the high-temperature oxidation resistance of this superalloy, allowing a considerable increase in the working temperature of this material.

The reason for such good behavior is evident from the metallographic images shown in Fig. 2, where the formation and subsequent growth of an Al_2O_3 barrier can be observed. An upper layer is present above the Al_2O_3 barrier, composed of a mixture of metallic oxides. Al_2O_3 scales grow by inward oxygen diffusion, while Cr_2O_3 and NiO scales grow by outward diffusion of Cr^{3+} and Ni^{2+} ions through the respective scales.[11] The upper layer has thus formed initially, prior to the development of the internal Al_2O_3 layer. Similar results have been reported in previous works on Al-containing alloys.[15–17] This external layer, in some cases, spalled from the sample during cooling to room temperature, but the process always stops at the barrier, which seems to be less affected by the heating/cooling cycles. The surface morphology after cooling suggests that the spallation process occurs by wedging, i.e., the oxide/substrate interface has a high adhesive strength relative to the cohesive strength of the oxide.[18] The presence of the Al_2O_3 barrier not only at the surface, but also at the substrate/melt-zone interface, indicates the importance of intergranular oxygen diffusion through the Incoloy substrate.[7] The absence of a dendritic zone in the region immediately below the barrier suggests that the dendrites have a high Al content, as is confirmed in the subsequent element maps of Figs. 4, 5, and 6. Al atoms from the dendrites move outwards to react with the incoming oxygen from the atmosphere and form the barrier. This mechanism ensures that, as long as the dendritic phase exists, there will be a supply of Al to form a protective Al_2O_3 layer.

Figure 3 shows a detail of the inner dendritic structure, which is similar to that found in other Ni–Cr–Al and Ni–Fe–Cr–Al systems with 10–15% Al.[16,17] According to the element maps of Figs. 4, 5, and 6, the dendritic zone would be composed of Ni–Al phases, whereas the matrix seems to be a solid solution of all four main elements. Some Cr aggregates start to form when oxidation time increases, as was also observed in previous work.[16,17] Additionally to the element maps, and to give some numerical data on the composition of each phase, X-ray fluorescence spectroscopy measurements were carried out by focusing the income electron beam (size $\leq$200 nm) on each zone, while recording the spectrum in the energy dispersive mode. The spectra were corrected to take into account self-absorption and autoionization effects, and the results are shown in Table I. The table gives the relative compositions, in atomic percent, of the different zones observed, which are numbered from 1 to 6. Zone 1 corresponds to the solid solution extending all over the melt zone. Its composition is not completely uniform, being different at the surface and interface regions with respect to the inner zone, and changing with oxidation time, as shown in the table. The lower Al-contents of the surface and interface regions are probably originated from the diffusion of Al-atoms from these regions towards the barrier, together

Table I. Relative Composition of the Different Observed Zones Obtained by X-Ray Fluorescence Analysis. The Data Are Given as Atomic Percent. A Description of Each Zone Can Be Found in the Text

	Al	Fe	Ni	Cr	Si	Ti
Zone 1, 25 hr	6.1±0.7	48.6±0.7	22.4±0.9	21.0±0.8	1.9±0.2	—
Zone 1, 25 hr, surface	1.8±0.5	50.2±2.7	24.9±1.9	21.2±0.9	2.0±0.4	—
Zone 1, 25 hr, interface	4.8±0.7	48.2±1.5	23.9±1.2	20.9±0.8	2.1±0.3	—
Zone 1, 100 hr	5.8±0.7	43.9±1.2	31.1±0.9	18.1±0.5	1.2±1.0	—
Zone 2	26.7±1.5	18.1±1.4	49.8±1.2	4.5±0.3	—	—
Zone 3, 25 hr	4.9±0.2	46.1±0.1	12.8±0.7	33.2±0.1	2.2±0.1	0.8±0.4
Zone 4, above barrier	50.4±1.0	19.9±0.4	9.7±0.7	12.6±0.4	3.9±0.6	3.2±0.6
Zone 4, barrier	89.0±1.2	4.4±0.1	2.6±0.8	2.3±0.1	—	1.8±1.0
Zone 4, below barrier	73.8±1.0	9.6±0.5	6.5±0.5	4.6±0.3	—	5.5±1.0
Zone 5	—	16.9±2.3	4.4±1.3	75.4±6.8	1.4±0.7	0±2
Zone 6	—	—	—	—	—	100

with Al-atoms from the dendritic phase, leading to an Al-depleted or precipitate-free zone. This effect is less pronounced at the interface than at the surface, due to the smaller thickness of the barrier in the former zone, probably induced by the lower oxygen flux. By increasing the oxidation time from 25 hr to 100 hr, the relative composition varies, decreasing the amount of Fe and Cr while that of Ni increases. Two mechanisms can be responsible for these changes: first, the migration of Fe and Cr atoms to the surface, above the barrier, to form the external metallic oxide layer; second, the incorporation of Ni atoms to the solid solution coming from the Ni–Al dendritic zone. As will be discussed below, this zone consists of a mixture of Ni_3Al and NiAl phases. A transformation of the Ni_3Al component into NiAl could lead to an excess of Ni which would diffuse towards the matrix.

Zones 2 and 3 correspond to the two different dendritic structures observed in Fig. 4. Whereas Zone 2, which corresponds to the Ni–Al phases, is present for all oxidation times, Zone 3 is only observed after 25 hr oxidation and, to a much lower extent, after 50 hr oxidation, disappearing for longer times. In both cases, no changes in the composition with position nor with oxidation time were observed. Zone 4 corresponds to the Al-rich aggregates, and three cases have been distinguished: the larger, elongated aggregates above the barrier, those at the barrier, and the smaller aggregates observed below the barrier in samples after long oxidation times. The first and third cases occur only in the surface regions, since at the interface only the aggregates forming the barrier are present. The most-external grains have the lowest Al content, and probably consist of mixed Al, Fe, and Cr oxides, similar to those found in similar systems.[12,15] The grains at the barrier are almost exclusively Al, in the form of Al_2O_3, confirming the high protective character of this layer. Finally, the grains below the barrier constitute

a previous stage of Al atoms before incorporation into the barrier, and consist of a mixture of Al and other minority phases. Note the high Ti content of these aggregates, which could indicate that small Ti grains serve as nucleation seeds for Al_2O_3 formation. These small Ti grains (phase 6) are uniformly distributed in all samples. The role of Si is not as clear, although some authors claim that it improves the corrosion resistance of the material.[11,15] In the present case, an increment in Si at the outermost oxide layer occurs, whereas at the barrier no Si is observed. Finally, Zone 5 corresponds to Cr-rich spherical aggregates which start to form after an oxidation time of 50 hr, increasing in number after longer times. Since Cr has a higher solubility in the γ phase (solid solution, Zone 1) than in the β and γ' phases (NiAl and Ni_3Al, Zone 2) these structures are expected to precipitate inside the dendritic phase, as is indeed the case. Similar intradendritic Cr-aggregates have also been found in other Ni–Cr–Al systems after high-temperature treatment.[19,20]

Contrary to Zones 4, 5, and 6, which correspond to almost pure phases (Al, Cr, and Ti, respectively), Zones 1, 2, and 3 seem to be composed of a mixture of different compounds. In order to identify the composition of these zones, an analysis based on three ternary equilibrium phase diagrams: Fe–Cr–Al, Ni–Cr–Al, and Fe–Ni–Al[21] has been carried out. This kind of analysis is not aimed to give an exact composition of the different zones, but it serves as a first approach to characterize a complex system like the present one. The results are shown in Table II. Components in italic are minor components or were found only at some positions in the sample. According to this table, Zone 1 corresponds to a solid solution of all three main elements plus Al, as was already pointed out. Some small aggregates of Ni_3Al and FeAl, not visible in the SEM images, could also be present, dissolved in this phase.[19] Zone 2 corresponds mainly to Ni–Al phases, such as NiAl and Ni_3Al, but also to Fe–Al phases, like FeAl; also some mixed compounds, such as $(Fe_xNi_{1-x})Al_y$, might be present. In other similar materials, a dendritic structure consisting of a γ phase (solid solution) as matrix and a γ' phase (Ni_3Al) as the dendritic phase, has previously been reported.[16] Finally, Zone 3 corresponds mainly to a CrFe phase which, as already

Table II. Results of an Analysis Based on the Ternary Equilibrium Phase Diagrams of the Main Components, i.e., Al, Fe, Cr, and Ni

	Al–Ni–Fe	Al–Ni–Cr	Al–Fe–Cr
Zone 1	(Fe, Ni) + *Ni_3Al*	(Ni) + (Cr) + *Ni_3Al*	(Cr, αFe) + *CrFe*
Zone 2	(Fe, Ni) + $(Fe_xNi_{1-x})Al_y$ + *Ni_3Al*	NiAl + Ni_3Al + (*Cr*)	FeAl + (*$Cr_{1-x}Fe_x)_2Al$* + *Cr_5Al_8* + (*Cr*, *αFe*)
Zone 3	(Fe, Ni)	(Cr) + *Ni_3Al* + (*Ni*)	(Cr, αFe) + CrFe

mentioned, is only visible in samples oxidized for short time periods, dissolving afterwards into the solid solution.

CONCLUSIONS

The oxidation resistance of laser-surface-alloyed Incoloy-800H with Al at 1000°C in air has been tested. Several samples have been oxidized for different time intervals between 25 hr and 1000 hr and investigated by optical microscopy, SEM, and X-ray fluorescence spectroscopy. After a first optical inspection the laser-treated material seems to have considerably increased its oxidation resistance with respect to the nontreated material. The reason for such an improvement is the formation of an Al-rich layer, in form of Al_2O_3, close to the surface, which acts as a barrier against oxygen diffusion into the bulk.

The inner part of the laser-treated zone has a dendritic structure, contrary to the equiaxed granular structure of the samples prior to oxidation. The dendritic grains increase in size with increasing oxidation time, and a dendritic-free region close to the Al-rich barrier is formed. The dendritic grains consist of a mixture of Ni–Al, Fe–Al, and Ni–Fe–Al intermetallic compounds whose main constituents are FeAl, NiAl, and Ni_3Al, whereas the matrix is a solid solution of all the main elements. The dendritic-free region near the barrier is formed due to the diffusion of Al atoms from the Al-rich dendrites towards the barrier, leading to a region with low Al content. Other phases also present are Cr-aggregates (α phase), Ti-aggregates, and a CrFe phase which is present only after low oxidation times.

In summary, laser-surface-alloyed Incoloy-800H with Al greatly improves the corrosion resistance of the base material due to an Al-rich barrier close to the surface, allowing to increase its working temperature considerably.

ACKNOWLEDGMENTS

The authors wish to thank V. López for his help during the metallographic characterization of the samples. This work has been supported by the Spanish Comisión Interministerial de Ciencia y Tecnología (CICYT), under project No. MAT93-0630C0201.

REFERENCES

1. G. W. Goward, *Mater. Sci. Technol.* **2**, 194 (1986).
2. R. W. Richards, R. D. Jones, P. D. Clements, and H. Clarke, *Int. Mater. Rev.* **39**, 191 (1994).
3. J. J. de Damborenea and A. J. Vázquez, *J. Mater. Sci.* **27**, 1271 (1992).

4. B. C. Oberländer and E. Lugscheider, *Mater. Sci. Technol.* **8**, 657 (1992).
5. J. Mazumder and J. Singh, in *Laser surface treatment of metals*, Vol. 115 of *NATO ASI Series E*, C. W. Draper and P. Mazzoldi eds. (Kluwwer Academic Publishers, Dordrecht, Boston, London, 1986), p. 297.
6. E. McCafferty and P. G. Moore, in *Laser Surface Treatment of Metals*, Vol. 115 of *NATO ASI Series E*, C. W. Draper and P. Mazzoldi eds. (Kluwer Academic Publishers, Dordrecht, Boston, London, 1986), p. 263.
7. J. de Damborenea, V. López, and A. J. Vázquez, *Surf. Coat. Technol.* **70**, 107 (1994).
8. W. Maocai and W. Weitao, *Surf. Coat. Technol.* **72**, 181 (1992).
9. J. H. Abboud and D. R. F. West, *Mater. Sci. Technol.* **7**, 353 (1991).
10. N. S. Stoloff, *Properties and selection: irons, steels, and high-performance alloys*, Vol. 1 of *Metals Handbook (10th Edition)* (ASM International, Ohio, 1990), p. 950.
11. G. C. Wood and F. H. Stott, *Mater. Sci. Technol.* **3**, 519 (1987).
12. S. Zhu, F. Wang, H. Low, and W. Wu, *Surf. Coat. Technol.* **71**, 9 (1995).
13. W. W. Steen, in *Laser surface treatment of metals*, Vol. 115 of *NATO ASI Series E*, C. W. Draper and P. Mazzoldi eds. (Kluwer Academic Publishers, Dordrecht, Boston, London, 1986), p. 369.
14. A. Gutiérrez and J. de Damborenea, *Appl. Phys. A.* to be published (1996).
15. S. Ghosh, A. Prodhan, O. N. Mohanty, and A. K. Chakrabarti, *Oxid. Metals* **45**, 109 (1996).
16. J. J. de Damborenea and A. J. Vázquez, *J. Mater. Sci.* **28**, 4775 (1993).
17. J. L. G. Carrasco, P. Adeva, and M. Aballe, *Oxid. Metals* **33**, 1 (1990).
18. H. E. Evans, *Inter. Mater. Rev.* **40**, 1 (1995).
19. J. L. González-Carrasco, P. Adeva, and M. Aballe, *Mater. Sci. Eng. A.* **128**, 231 (1990).
20. W. F. Gale, T. C. Toteimer, and J. E. King, *Metal. Mater. Trans. A* **26**, 949 (1995).
21. *Ternary Alloys*, G. Petzow and G. Effenberg, eds. (VCH, Weinheim, Germany, 1991), Vol. 3, p. 369; ibid p. 400; ibid Vol. 4, p. 309.